Optics Design of the Multi-color TES Bolometer Camera for the ASTE Telescope

Tatsuya Takekoshi, Tetsuhiro Minamidani, Shunichi Nakatsubo, Tai Oshima, Masayuki Kawamura, Hiroshi Matsuo, Tatsuhiro Sato, Nils W. Halverson, Adrian T. Lee, William L. Holzapfel, Yoichi Tamura, Akihiko Hirota, Kenta Suzuki, Takuma Izumi, Kazuo Sorai, Kotaro Kohno and Ryohei Kawabe

***Abstract*—Wideband and high spatial resolution continuum observations in the millimeter and submillimeter wavelengths are of great importance to understand star formation history of galaxies from distant to nearby (early to recent universe), and thermal and non-thermal aspects of clusters of galaxies through Sunyaev-Zel'dovich effect. To promote such studies based on the millimeter and submillimeter continuum data, new TES (Transition Edge Sensor) bolometer camera for the ASTE telescope has been developed. We aim to observe three bands, 1100μm, 850μm and 450μm. Camera optics is designed by geometrical optics to fit into the Cassegrain system of the ASTE telescope and the spatial limitation of its receiver cabin. For the efficient observation, our optics realizes 7.5' field of view and 2-band simultaneous observation. The two focal planes can accommodate two of three TES bolometer wafers which have 169, 271, and 881 pixels at 1100, 850, and 450μm, respectively. The camera optics is accomplished diffraction limited optics, which is confirmed from spot diagrams and strehl ratios. It is evaluated via physical optics calculation, and all pixels on each focal plane have aperture efficiency of $\sim$30% in absence of reflection and absorption loss by filters and the Ruze loss. The dimensions of the optical elements are also determined based on the results of the physical optics calculations.**

I. INTRODUCTION

IT is of great importance in astronomy and astrophysics to understand star formation history of galaxies from distant to nearby (from early to recent universe), and the evolution of large scale structure. Distribution and star formation rate of (sub)millimeter-bright galaxies (SMGs) are clues of galaxy evolution and the cosmic star formation history. Ultra-high temperature component of clusters of galaxies is also a clue to large scale structure formation history, because that component may be caused by collisions of clusters of galaxies that heat up surrounding materials.

Observations using AzTEC [1] on the ASTE telescope provided large map more than 1 deg^2 as deep as 0.5–1 mJy/beam, and more than 1000 sources were detected in the 1.1 mm wavelength [2]–[5]. Surveying SMGs, and determination of their redshifts and star formation rates is one of the immediate purposes of this project. Understandings of dust nature of nearby galaxies and the Milky Way is also important to reveal properties of not only themselves but also SMGs. The detection of ultra-high temperature components of clusters of galaxies through the Sunyaev-Zel'dovich (SZ) effect is another approach to understand the history of the large structure formation. Therefore, we aim to develop a new millimeter and submillimeter bolometer camera for the ASTE telescope and conduct large area surveys in the millimeter and submillimeter wavelengths.

The ASTE telescope [6], [7] is a 10-m submillimeter telescope (Figure 1) located at the Atacama Desert, Chile. Its altitude is 4850m and it is known as one of the best sites for submillimeter observations because of its good atmospheric transmission [8]. With this telescope, we aim to observe 1100 μm (270 GHz), 850 μm (350 GHz) and 450 μm (670 GHz) Bands. These bands are essentially important to determine photometric redshifts and star formation rates of distant galaxies, to understand dust nature in galaxies and the Milky Way, and to detect ultra-high temperature components of clusters of galaxies through the SZ effect. The bandwidths are determined as wide as possible avoiding the water vapor absorptions to achieve good sensitivities. Frequency bands, ranges, and bandwidths are summarized in Table I. Simultaneous observation capability of two or three bands and a large FoV at least 7.5 arcminutes diameter are necessary to achieve large area surveys within a reasonable project duration.

It is necessary to design and develop the optics to couple the TES bolometers to the Cassegrain optics of the ASTE telescope. In this paper, the optics design and design procedure for this camera is described.

II. OPTICS DESIGN

Under the scientific requirements and limitations mentioned above, we designed the optics system that couples to the Cassegrain system of the ASTE telescope whose antenna parameters are summarized in Table II. The ASTE telescope has a classical Cassegrain optics whose F-number is 8.878.

T. Takekoshi is with Department of Cosmosciences, Graduate School of Science, Hokkaido University, N10W8, Kita-ku, Sapporo, 060-0810, Japan e-mail: takekoshi@astro1.sci.hokudai.ac.jp.

T. Takekoshi, T. Oshima. M. Kawamura T. Sato, Y. Tamura, A. Hirota and R. Kawabe are with Nobeyama Radio Observatory.

T. Takekoshi, T. Oshima. M. Kawamura, H. Matsuo, T. Sato, Y. Tamura, A. Hirota and R. Kawabe are with National Astronomical Observatory of Japan.

T. Minamidani and K. Sorai are with Department of Physics, Faculty of Science, Hokkaido University.

S. Nakatsubo is with Institute of Low Temperature Science, Hokkaido University.

M. Kawamura, Y. Tamura, K. Suzuki, T. Izumi and K. Kohno are with Institute of Astronomy, The University of Tokyo.

N.W. Halverson is with Center for Astrophysics and Space Astronomy, University of Colorado.

N.W. Halverson is with National Institute of Standards and Technology.

A.T. Lee and W.L. Holzapfel are with Department of Physics, University of California.

A.T. Lee is with Physics Division, Lawrence Berkeley National Laboratory.

Fig. 1. Front and side view of the ASTE telescope. The Cassegrain system consists of a 10-m main-reflector and a 620-mm sub-reflector. The receiver cabin and the Cassegrain system move together with the elevation angle.

TABLE I
OBSERVING BANDS OF NEW BOLOMETER CAMERA FOR ASTE

Bands	Frequency range (GHz)	Band width (GHz)
270 GHz Band	244–294	50
350 GHz Band	330.5–365.5	35
670 GHz Band	630–710	80

The Cassegrain focus is located above the ceiling of the receiver cabin, and then rays reflected by the main- and sub-reflectors go into the receiver cabin with outspreading. Thus, it is necessary to set a re-imaging mirror in the receiver cabin.

The size of the receiver cabin is approximately 1.9 m in length $\times$ 2.2 m in width $\times$ 1.8 m in height, and a 19-inch standard rack occupies some space in the receiver cabin. All the optics components and the cryostat should be fit inside.

Figure 2 shows the position and design of the third mirror in the ASTE cabin. The re-imaging mirror is designed as an ellipsoidal mirror to refocus the outspreading rays into a focal plane in the cryostat. Because of the limitation described above, this ellipsoidal mirror is put at very close to the floor of the receiver cabin, and its aperture diameter becomes 560 mm to achieve 7.5 arcminutes FoV. This is the maximum size realized under the limitations of the available receiver cabin space. The preliminary ellipsoidal mirror causes large aberrations especially at the edges of the field of view, and modification is necessary to realize the diffraction-limited performance over the whole field of view and all frequency bands. We optimize the shape of the third mirror by addition of fifth order polynomials.

TABLE II
ANTENNA PARAMETERS OF ASTE

Main-reflector dia.	10 m
Sub-reflector dia.	620 mm
F/#	8.878
Surface accuracy	19 μm r.m.s.
Mainbeam efficiency	0.6-0.7 (850 μm)
Beam size	22” (850 μm)
Pointing accuracy	2” r.m.s.

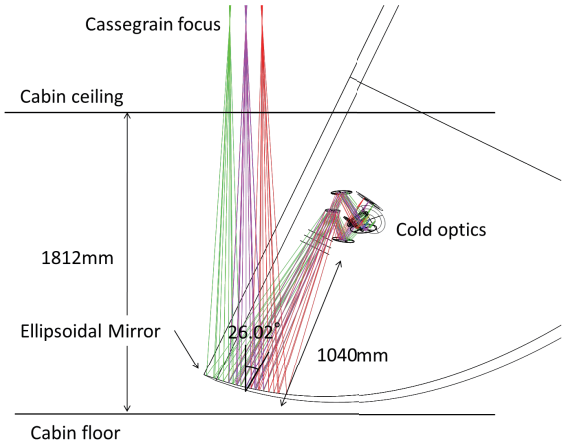

Fig. 2. Side view of the receiver cabin and optics cut along the reflected direction by ellipsoidal mirror. The ray from the Cassegrain system focuses near the ceiling of the receiver cabin.

The cryostat window is placed at a certain position to avoid the interference with rays between the sub-reflector and the re-imaging ellipsoidal mirror. This position limits the size of the cold optics to about a cube 500 mm on a side.

Inside of the cryostat, incident rays are divided into two bands using a dichroic filter. This is a key component to realize simultaneous multi-color optics without reducing the observing efficiency. This dichroic filter is placed at the pupil to reduce the filter aperture size, and inclines at 25 degree to the incident principle ray to keep good transmission and reflection characteristics. This makes it difficult to design an optics system that realizes simultaneous three bands observations, and we choose the design for the simultaneous two bands observations. Hereafter, we call the reflected band as “Band 1” and transmitted band as “Band 2”. We use these bands as 270 and 350 GHz Bands, respectively, for Phase I configuration, and 670 and 350 GHz Bands, respectively, for Phase II configuration. The cold Lyot stop, which reduces unexpected optical load to bolometers, is also placed at the pupil.

The numbers of pixels of each bolometer wafer are 271, 271, and 881 pixels for 270, 350, and 670 GHz Bands, respectively and the number of readouts is limited to $\sim$400 pixels for the Phase I (270 and 350 GHz Bands) operation. Therefore, we use the only central 169 pixels of 270 GHz Band wafer. This is because the sensitivity of 350 GHz Band is worse than that of 270 GHz Band due to the differences of atmospheric transmissions and detector bandwidths, and we assign as many pixels as possible for 350 GHz Band. The diameter of the central 169 pixels of the 270 GHz Band wafer corresponds to 55 mm, and we modify the shape and position of dielectric lens to keep the FoV of 7.5 arcminutes diameter. As a result, the numbers of pixels are 169, 271, and 881 pixels for 270, 350, and 670 GHz bands, respectively. All bands cover the FoV of 7.5 arcminutes diameter.

Figure 3 shows the final design of the cold optics. The rays split by the dichroic filter are reflected by plane mirrors respectively to make a compact cold optics. In each band,

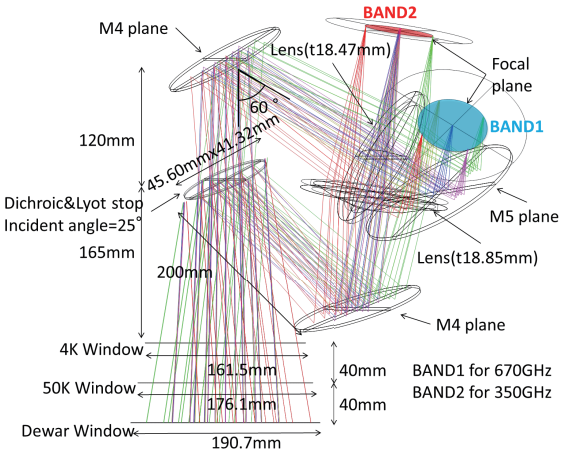

Fig. 3. Side view of Phase II cold optics cut along the reflected direction by the third mirror. The ray reflected by the third mirror goes through the 300 K, 50 K, and 4 K windows. The dichroic filter divides incoming rays into two bands, and each ray are focused after flat mirrors and HDPE lenses.

TABLE III
STREHL RATIOS AT EACH BAND AND FIELD

Field (dAZ, dEl)	270 GHz	350 GHz	670 GHz
1 (0', 0')	0.982	0.987	0.950
2 (-3.25', 1.13')	0.978	0.979	0.923
3 (3.25', -1.13')	0.998	0.995	0.984
4 (-1.13' ,-3.25')	0.979	0.969	0.892
5 (1.13' , 3.25')	0.977	0.966	0.883

dielectric lens is placed between the dichroic filter and a horn array to make a telecentric system and to fit the size of focal plane. For Band 1, an additional flat mirror is used between the dielectric lens and the horn array.

Imaging quality of this optics is checked using spot diagrams and Strehl ratios at 49 positions of each focal plane. We measured at 4 grids and 12 grids in radial and circumferential directions, respectively, and the center position. Table III shows the Strehl ratios of the five representative positions, corresponds to the center and the four edges fields. Strehl ratio of more than 0.8 is usually considered as diffraction limited, and we follow this criterion. They are all more than 0.8, and it is confirmed that designed optics achieves diffraction limited.

III. PHYSICAL OPTICS EVALUATION

The evaluations of the optics system under the geometrical optics assumptions are in good agreement with the actual in the short wavelengths (high frequencies). However, in the millimeter and submillimeter wavelengths, which are similar to the dimensions of optical elements, it is necessary that analysis considering the effects of the diffraction and interference. We use the Physical Optics (PO) antenna analysis software GRASP9 developed by TICRA for this analysis. PO is the method to solve the propagation of electromagnetic waves based on the Maxwell's equations. The current distribution of a scatterer's surface can be calculated from the beam pattern

TABLE IV
PARAMETERS OF BEAM PATTERNS AT EACH BAND AND FIELD

270 GHz	Field1	Field2	Field3	Field4
Gain (dBi)	84.63	84.71	84.07	84.54
Aperture efficiency (%)	36.33	37.00	31.92	35.54
FWHM minor (arcsec)	27.58	27.35	29.95	27.82
FWHM major (arcsec)	28.72	28.30	28.82	28.48
Sidelobe level (dB)	-17.87	-16.50	-17.29	-17.80
Cross pol. level (dB)	-34.62	-34.61	-34.79	-29.02

350 GHz	Field1	Field2	Field3	Field4
Gain (dBi)	86.91	86.89	86.28	86.74
Aperture efficiency (%)	36.50	36.39	31.61	35.15
FWHM minor (arcsec)	21.29	21.25	23.13	21.54
FWHM major (arcsec)	22.14	21.83	22.36	22.02
Sidelobe level (dB)	-17.58	-16.16	-17.45	-17.45
Cross pol. level (dB)	-33.89	-34.26	-34.34	-28.72

670 GHz	Field1	Field2	Field3	Field4
Gain (dBi)	92.23	92.22	91.47	91.69
Aperture efficiency (%)	33.95	33.89	28.50	29.99
FWHM minor (arcsec)	11.14	10.85	12.12	11.37
FWHM major (arcsec)	11.51	11.52	11.68	11.61
Sidelobe level (dB)	-16.89	-15.34	-17.09	-14.77
Cross pol. level (dB)	-35.02	-35.08	-35.15	-28.46

The tables are the cases of 85% diameter of the geometrical cold Lyot stop and no horn offset.

of the previous scatterer, which is calculated by the current distributions on the previous scatterer.

We make the equivalent model of the designed optics described in Section II, which includes the main-reflector, the sub-reflector, the third mirror, the 300 K cryostat window, the 50 K shield window, the 4 K shield window, the cold Lyot stop (dichroic filter), the fourth flat mirror, the dielectric lens, the fifth flat mirror, and the conical horn. All these optical elements except the conical horn are modeled as reflective mirrors with the same aperture size as designed because of their ease to use. A dielectric lens is modeled as a spherical reflector under the assumptions of a thin lens and a telecentric optics. Optical components that limit the diameter of the beams, that is, cold Lyot stop, 4 K and 50 K shields, and cryostat windows, are modeled as plane mirrors with the appropriate aperture size. Additionally, the blockage of the sub-reflector is treated as a hole on the main-reflector, and the blockage of the sub-reflector supporting structure is neglected. As the surfaces of optical elements are assumed to be perfect, Ruze losses are neglected.

Spillovers of each optical element are also provided from the each run. We assumed that these spillovers are terminated to the certain temperature (4 K or 300 K), and estimate the photon noise originated from the optics in the form of noise equivalent power (NEP). We adopt the cold stop diameter of 85% of geometrical design because photon noise from optics is minimized. PO calculation provides us beam patterns of E-plane, H-plane, and cross polarization (Figure 4), then some beam parameters, that is, gain, beam size (FWHM), sidelobe level, and cross polarization level are obtained. Those results are summarized in Table IV.

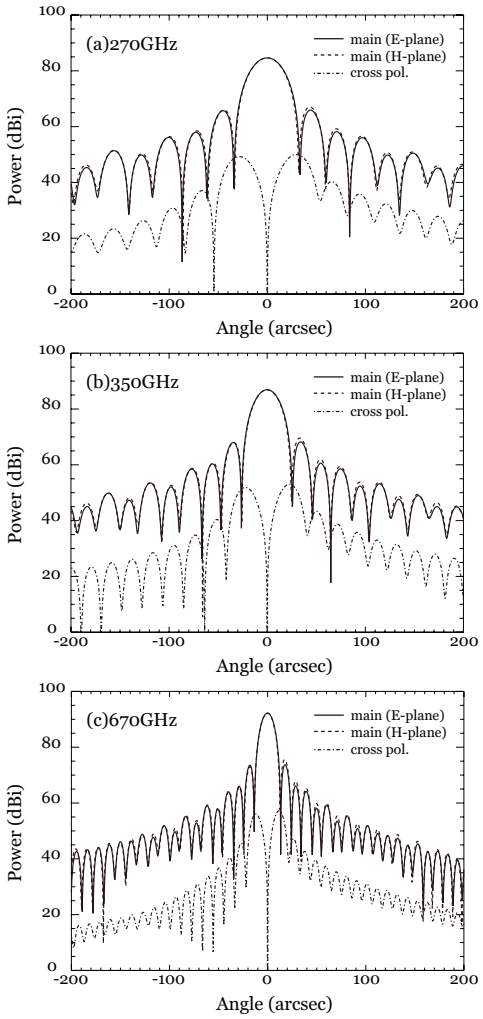

Fig. 4. Beam patterns of the central beam (Field 1) of (a) 270 GHz, (b) 350 GHz, and (c) 670 GHz Bands. These are the cases of 85% diameter of the geometrical cold Lyot stop and no horn offset.

IV. Summary

We designed the optics of multi-color TES bolometer camera for the ASTE telescope. The designed optics fitted inside of the ASTE cabin and the camera cryostat. The optics for 2-color simultaneous observation and 7.5 arcminutes diameter FoV were achieved. We will operate 270 GHz and 350 GHz Bands for Phase I configuration, and 350 GHz and 670 GHz Bands for Phase II configuration. The numbers of pixels were optimized in terms of mapping speed and they became 169, 271, and 881 pixels for 270, 350, and 670 GHz Bands, respectively.

We evaluated the designed optics using physical optics (PO) method. And we adopted the cold stop diameter of 85% of geometrical design because photon noise from optics was minimized. As a result of optimization, aperture efficiencies of each beam were $\sim$ 30% at each band. Beam sizes (FWHM) were $\sim$ 28 arcseconds, 22 arcseconds, and 12 arcseconds, for 270 GHz, 350 GHz, and 670 GHz Bands, respectively.

Acknowledgment

We are deeply grateful to Tom Nitta who provided the scripts for the data analysis of FTS measurements. A part of this work is financially supported by MEXT Grant-in-Aid for Specially Promoted Research (20001003). Tatsuya Takekoshi gratefully appreciates the financial support by the Clark fellowship of Hokkaido University.

References

[1] G. W. Wilson, J. E. Austermann, T. A. Perera, K. S. Scott, P. A. R. Ade, J. J. Bock, J. Glenn, S. R. Golwala, S. Kim, Y. Kang, D. Lydon, P. D. Mauskopf, C. R. Predmore, C. M. Roberts, K. Souccar, and M. S. Yun, "The AzTEC mm-wavelength camera," MNRAS, vol. 386, p. 807, 2008.

[2] Y. Tamura, K. Kohno, K. Nakanishi, B. Hatsukade, D. Iono, G. W. Wilson, M. S. Yun, T. Takata, Y. Matsuda, T. Tosaki, H. Ezawa, T. A. Perera, K. S. Scott, J. E. Austermann, D. H. Hughes, I. Aretxaga, A. Chung, T. Oshima, N. Yamaguchi, K. Tanaka, and R. Kawabe, "Spatial correlation between submillimetre and Lyman-α galaxies in the SSA22 protocluster," Nature, vol. 459, p. 61, 2009.

[3] K. S. Scott, M. S. Yun, G. W. Wilson, J. E. Austermann, E. Aguilar, I. Aretxaga, H. Ezawa, D. Ferrusca, B. Hatsukade, D. H. Hughes, D. Iono, M. Giavalisco, R. Kawabe, K. Kohno, P. D. Mauskopf, T. Oshima, T. A. Perera, J. Rand, Y. Tamura, T. Tosaki, M. Velazquez, C. C. Williams, and M. Zeballos, "Deep 1.1mm-wavelength imaging of the GOODS-S field by AzTEC/ASTE - I. Source catalogue and number counts," MNRAS, vol. 405, p. 2260, 2010.

[4] B. Hatsukade, K. Kohno, I. Aretxaga, J. E. Austermann, H. Ezawa, D. H. Hughes, S. Ikarashi, D. Iono, R. Kawabe, S. Khan, H. Matsuo, S. Matsuura, K. Nakanishi, T. Oshima, T. Perera, K. S. Scott, M. Shirahata, T. T. Takeuchi, Y. Tamura, K. Tanaka, T. Tosaki, G. W. Wilson, and M. S. Yun, "AzTEC/ASTE 1.1-mm survey of the AKARI Deep Field South: source catalogue and number counts," MNRAS, vol. 411, p. 102, 2011.

[5] S. Ikarashi, K. Kohno, J. E. Aguirre, I. Aretxaga, V. Arumugam, J. E. Austermann, J. J. Bock, C. M. Bradford, M. Cirasuolo, L. Earle, H. Ezawa, H. Furusawa, J. Furusawa, J. Glenn, B. Hatsukade, D. H. Hughes, D. Iono, R. J. Ivison, S. Johnson, J. Kamenetzky, R. Kawabe, R. Lupu, P. Maloney, H. Matsuhara, P. D. Mauskopf, K. Motohara, E. J. Murphy, K. Nakajima, K. Nakanishi, B. J. Naylor, H. T. Nguyen, T. A. Perera, K. S. Scott, K. Shimasaku, T. Takagi, T. Takata, Y. Tamura, K. Tanaka, T. Tsukagoshi, D. J. Wilner, G. W. Wilson, M. S. Yun, and J. Zmuidzinas, "Detection of an ultrabright submillimetre galaxy in the Subaru/XMM-Newton Deep Field using AzTEC/ASTE," MNRAS, vol. 415, p. 3081, 2011.

[6] H. Ezawa, R. Kawabe, K. Kohno, and S. Yamamoto, "The Atacama Submillimeter Telescope Experiment (ASTE)," in *Proc. of SPIE*, vol. 5489, 2004, p. 763.

[7] H. Ezawa, K. Kohno, R. Kawabe, S. Yamamoto, H. Inoue, H. Iwashita, H. Matsuo, T. Okuda, T. Oshima, T. Sakai *et al.*, "New achievements of ASTE: the Atacama Submillimeter Telescope Experiment," in *Proc. of SPIE*, vol. 7012, 2008.

[8] S. Matsushita, H. Matsuo, J. R. Pardo, and S. J. E. Radford, "FTS Measurements of Submillimeter-Wave Atmospheric Opacity at Pampa la Bola II : Supra-Terahertz Windows and Model Fitting," PASJ, vol. 51, p. 603, 1999.

Tatsuya Takekoshi was born in Hokkaido, Japan in 1985. He received the degrees of B.S. in Physics and M.S in Cosmoscience from Hokkaido University, Sapporo, Japan in 2008 and 2010, respectively. His current research interests are development of the multi-color TES bolometer camera for the ASTE telescope, and an observational study of starformation process in the low metallicity environment using millimeter and submillimeter instruments.